Mn-porphyrins Anchored onto Magnetic Nanoparticles via Different Linker Length: A Comparative Study in Aerobic Oxidation of Olefins

Saeed Rayati (rayati@kntu.ac.ir)
https://orcid.org/0000-0003-2941-7216
Saeedeh Shokoohi

Research Article

Keywords: Magnetic nanoparticles, Manganese porphyrin, Epoxidation, Molecular oxygen, Different linker

Posted Date: March 30th, 2022

DOI: https://doi.org/10.21203/rs.3.rs-1476238/v1

Abstract

In this research, *meso*-tetrakis(4-carboxyphenyl)porphyrinatomanganese(III) acetate has been immobilized onto the modified silica-coated Fe_3O_4 nanoparticles with linkers with different chain lengths (short, Fe_3O_4@SiO_2-MnTCPP (C-1), medium Fe_3O_4@SiO_2-NH_2-MnTCPP (C-2), and long length, Fe_3O_4@SiO_2-NHCO-NH_2-MnTCPP (C-3)). The catalysts were characterized by various analytical and spectroscopic methods, including FT-IR, UV-Vis, XRD, FE-SEM, TEM, TGA, and VSM. A comparative study based on the difference in chain length of the linker in the oxidation of olefins with molecular oxygen was performed. The novel linker (long-chain catalyst) was designed to improve the performance of the catalytic activity (complete conversion of the α-methyl styrene, 4-methyl styrene and 4-chloro styrene was achieved after 2 h). The new heterogenized catalyst (Fe_3O_4@SiO_2-NHCO-NH_2-MnTCPP) not only shows higher catalytic activity in the oxidation of different olefins, but also shows better reusability of the catalyst.

1 Introduction

Today, oxidation reactions have a substantial role in modern chemistry as well as the chemical industry [1]. From the point of view of green chemistry, selective oxidation reaction with non-toxic oxidants is valuable. The use of green oxidants such as hydrogen peroxide, urea hydrogen peroxide, molecular oxygen, and air in the catalytic oxidation systems have become favored [2, 3]. Among the green oxidants, molecular oxygen particularly attracted considerable attention. Low cost, high active oxygen content, and the absence of by-products are significant advantages of molecular oxygen. Although molecular oxygen is an impressive oxidant, but it should be activated by a reducing agent such as isobutyraldehyde [4–8].

In organic synthesis, olefins oxidation reactions can be used to produce essential precursors, including alcohols, epoxides, and aldehydes [9]. Among these compounds, epoxidesare the most valuable and versatile intermediates for the manufacturing of fine chemicals such as plasticizers, perfumes, cosmetics, epoxy resins, pharmaceuticals, etc. [10–12]. Aim to achieve epoxides with great yield and selectivity, oxidation of olefins can be commonly mediated with transition metal complexes as catalyst in homogeneous and heterogeneous catalytic systems [13–16]. Metalloporphyrins are a well-known class of metal complexes which mimic the cytochrome P-450 enzyme in oxidation reactions of metabolic processes [17–19]. Although the catalytic reactions in the homogeneous systems regard to their large surface area show high activity, the application of homogeneous catalysts are limited due to their drawbacks. The tedious workup and recycling of the catalysts, contaminated product, high cost, and difficulty in separation are some undesirable points [20–22]. To overcome these difficulties, the heterogenization of a homogeneous catalyst onto solid supports can be impressive. Nowadays, much attention has been allocated to the application of materials as solid supports for preparation of heterogeneous catalysts [23–26]. Through many types of support, immobilization of transition metal complexes to the surface of nanosheets, nanotubes, and nanomaterials, especially magnetic nanoparticles, attracted more attention. The magnetic nanoparticles like Fe_3O_4, due to their advantages

such as low cost, chemical and high thermal stability, non-toxic, strong magnetization, and easy separation would be the most beneficial candidate for functionalization of complexes [27–29]. Herein, in accordance with green chemistry importance and application of epoxies, Mn-porphyrin immobilized onto the surface of magnetic nanoparticles (MNPs) with different linker lengths and used for oxidation of different olefins with molecular oxygen.

2 Experimental

2.1 General Remarks

All chemicals and solvents applied in the current study prepared from Merck or Aldrich with the commercially available highest grade. All of reagents were used or stored in a proper place without any further purification. UV-Vis spectra were assessed with a Lambda 25 Perkin Elmer spectrophotometer in a range of 300–800 nm. The Fourier transform infrared (FT-IR) spectra were recorded as KBr pellets using an ABB Bomem: FTLA 2000 – 100 in the range of 400–4000 cm^{-1}. Manganese content was determined by using a PR-5 Shimadzu atomic absorption spectrometer. The morphology features of solid samples were investigated by transmission electron microscopy (TEM) using Zeiss-EM10C-100kV (Germany). Field emission scanning electron microscopy (FE-SEM) was done using a Zeiss-Sigma VP (Germany). Powder X-ray diffraction patterns were collected at an STOE diffractometer with wavelength 1.5406 Å (Cu Kα) at 40 kV and 40 mA supplied current. The thermal stability of samples was assessed by the thermal gravimetric analysis (Rheometric scientific-STA 1500). Magnetic properties of materials determined on an MDKB vibrating sample magnetometer (VSM) at room temperature. The product's purity detection was carried out by GC-FID on an Agilent 7890B instrument using a SAB-5 capillary column with phenyl methyl siloxane 30m × 0.32 mm × 0.25 μm.

2.2 Preparation of MnTCPP complex

The free-base porphyrin (*meso*-tetrakis(4-carboxyphenyl)porphyrin, H_2TCPP), and its manganese complex (MnTCPP) were prepared according to the procedure described in the literature [30, 31].

2.3 Preparation of Fe_3O_4@SiO_2

Preparation of Fe_3O_4 was carried out using a previously reported method [28]. Silica is an inert coating material which prevents the aggregation of the superparamagnetic core. Therefore, to improve the stability of magnetic nanoparticles and also provides a scaffold for the attachment of different functional groups, the surface of the prepared magnetic particles will be coated with silica. To prepare Fe_3O_4@SiO_2 microspheres, Fe_3O_4 particles (0.5 g) dispersed in the mixture of ethanol and ammonia solution (25%) under ultrasonic irradiation for 15 minutes, followed by the addition of tetraethyl orthosilicate (TEOS) and reaction mixture refluxed for 12 h. The resulting particles were collected using a magnet and washed with ethanol and ultra-pure water several times and dried at 60 ℃ [32].

2.4 Preparation of Fe_3O_4@SiO_2-NH_2

Fe_3O_4@SiO_2 (0.7 g) was dispersed in distilled water for 15 minutes. Aim to functionalize the surface of nanoparticles, 3 ml of (3-aminopropyl)triethoxysilane (APTES) were then added, and the mixture was stirred for 6 h at 80 ℃. The resulting particles were separated and suspended in 30 ml ethanol by ultrasonication for 10 minutes. Finally, the particles were washed several times with deionized water and dried at 60 ℃ [28, 33].

2.5 Preparation of Fe_3O_4@SiO_2-NHCO-NH_2

In order to increase the length of linker, 4-aminobutyric acid has been used. First, amine group of 4-aminobutytic acid should be protected with N-(9H-Fluoren-9-ylmethoxycarbonyloxy)succinimide (Fmoc-OSu). Briefly, Fmoc-OSu (0.5 g) in ethyl acetate (2 ml) was added to a mixture of 4-aminobutyricacid (0.2 g) and sodium carbonate in water, and the reaction mixture was stirred at room temperature for 48 hours. The progress of the reaction was monitored using TLC. At the end of the reaction, the precipitate was filtered by rotary (SI. 1 a,b) [34, 35].

Protected 4-aminobutyric acid was anchored onto the surface of amine-functionalized magnetic nanoparticles (Fe_3O_4@SiO_2-NH_2) through covalent linkage. The carboxyl group of the 4-aminobutyric acid was attached to the -NH_2 group of magnetic nanoparticles (Fe_3O_4@SiO_2-NH_2) using 2-(1H-benzotriazole-1-yl)-1,1,3,3-tetramethyluronium tetraflouroborate (TBTU) and in the presence of N,N'-diisopropylethyl amine (DIPEA). A strong external magnet was collected the supported magnetic nanocatalyst and repeatedly washed with DMF and ethanol and dried at 55°C for 18 h. The Fmoc group was removed by adding piperidine in DMF (25%) (14 ml) to the vessel and shaking the mixture for 30 min. Finally, the brown powder was washed with DMF and EtOH, and dried at oven 50℃ [34, 36].

2.6 Preparation of nano catalyst (Fe_3O_4@SiO_2-NHCO-NH_2 - MnTCPP)

For nanocatalyst synthesis, MnTCPP (0.7 mmol) was dissolved in 40 ml DMF. The prepared solid support (Fe_3O_4@SiO_2-NHCO-NH_2) (1 g), TBTU (0.41 g), and DIPEA (0.3 g) were added to the mixture and stirred for 48 hours at room temperature [34, 37]. The new magnetic nanocatalyst was collected by external magnet, washed with DMF and EtOH to remove unreacted reagents, and dried at 55 ℃ for 24 hours.

Aim to comparative study, both Fe_3O_4@SiO_2-MnTCPP (C-1) (MnTCPP complex was anchored directly to the silica-coated surface of magnetic nanoparticles) and Fe_3O_4@SiO_2-NH_2-MnTCPP (C-2) (MnTCPP was immobilized onto the surface of amine functionalized magnetic nanoparticles) have been prepared according to the previous procedure [16, 28].

2.7 General procedure for oxidation of olefins

To carry out the catalytic experiments, in 5ml test tube, 0.0015 mmol of the prepared nanocatalyst, 0.15 mmol of alkene, and 0.75 mmol of isobutyraldehyde (IBA) were added in 1 ml acetone. The oxidation reaction was started under molecular oxygen atmosphere (O_2 balloon) and stirred for 2 h at an

appropriate temperature. After completion of the reaction, the heterogeneous nanocatalyst was magnetically recovered, and the organic phase was analyzed by GC-FID, and the oxidation product was identified by comparison with authentic samples.

3 Results And Discussion

The stepwise long-chain heterogeneous catalyst (Fe_3O_4@SiO_2-NHCO-NH_2-MnTCPP (C-3)) preparation route is given in Scheme 1. Also C-1, and C-2 catalysts are presented in Fig. 1. The designed nanocatalysts were fully characterized by different standard methods.

3.1 Characterization of magnetic nanocatalysts

The amount of immobilized manganese onto the support surface was evaluated via atomic absorption spectroscopy (AAS). Based on the results, each gram of Fe_3O_4@SiO_2-MnTCPP, Fe_3O_4@SiO_2-NH_2-MnTCPP, and Fe_3O_4@SiO_2-NHCO-NH_2-MnTCPP contain 621, 635, and 265 µmol of MnTCPP complex respectively.

The FT-IR characterization for Fe_3O_4@SiO_2-MnTCPP, Fe_3O_4@SiO_2-NH_2, Fe_3O_4@SiO_2-NH_2-MnTCPP, Fe_3O_4@SiO_2-NHCO-NH_2, and Fe_3O_4@SiO_2-NHCO-NH_2-MnTCPP are presented in Fig. 2. The absorption bands at 469 cm^{-1} and 643 cm^{-1} are related to the Fe-O vibration in Fe_3O_4, which detected in all catalysts (Fig. 2. a-e) [38]. The antisymmetric and symmetric stretching bands associated with Si-O-Si (in all catalysts) were presented at 1098 cm^{-1} and 798 cm^{-1}, respectively (Fig. 2. a-e) [39]. Also, the sharp absorption bands at 1631 cm^{-1} and 3429 cm^{-1} confirmed the presence of the amino group (Fig. 2. a). An intense peak at 1658 cm^{-1} verified the amidic bond onto the surface of Fe_3O_4@SiO_2-NHCO-NH_2 (Fig. 2. b) [28]. The new absorption bands at 1653 and 1641 cm^{-1} are related to the formation of amide bond in the reaction between carboxyl groups (-COOH) of metalloporphyrin and amine groups (-NH_2) of the magnetic support correspond to Fe_3O_4@SiO_2-NH_2-MnTCPP and Fe_3O_4@SiO_2-NHCO-NH_2-MnTCPP (Fig. 2. c, d) [40]. In addition, in Fig. 2e, the signal at 1650 cm^{-1} could be assigned to the formation of a steric bond between –COOH groups of manganese porphyrins and -OH groups of the Fe_3O_4@SiO_2 [16, 41]. The other peaks at the region of 1397 cm^{-1} are in agreement with the vibrations of metalloporphyrin [42, 43].

The UV-Vis spectra of dispersed H_2TCPP, MnTCPP, C-1, C-2, and C-3 in DMF exhibit Soret band of Mn-porphyrin (Fig. 3. a, b, d, e, f), while no absorption band was observed for Fe_3O_4@SiO_2-NHCO-NH_2 (Fig. 3. c). A typical Soret and Q-bands of free base H_2TCPP are detectable in Fig. 3. a. In the UV-Vis spectra of MnTCPP, a Soret band with high intensity at 469 nm and two weaker Q-bands at 574 and 612 nm appeared (Fig. 3. b). The red-shift of the Soret band was occurred after deposition of MnTCPP on the surface of magnetic support for all catalysts which recorded at 486, 485 and 481 nm for Fe_3O_4@SiO_2-MnTCPP, Fe_3O_4@SiO_2-NH_2-MnTCPP, and Fe_3O_4@SiO_2-NHCO-NH_2-MnTCPP respectively (Fig. 3. d, e, f). The red-shift of the Soret bands may be due to the aggregation of Mn-porphyrin onto the surface of solid supports [16, 44, 45].

The obtained results from FT-IR, UV-Vis, and AAS strongly confirmed the immobilization of manganese porphyrin onto the surface of nanomagnetic supports.

The X-ray diffraction pattern in the 2θ range of 5 to 80° has been recorded to investigate the crystalline structure of all heterogeneous catalysts (Fig. 4). Some characteristic peaks at 30, 35, 44, 53, 57, and 62 degrees correspond to (220), (311), (400), (422), (511), and (440) plans of cubic inverse spinel Fe_3O_4. All of the observed diffraction peaks are in good agreement with the database in JCPDS file [28]. The results confirmed the stability and crystalline structure of silica-coated MNPs during the subsequent modification (Fig. 4. a-g). The average particle size has been estimated using Debye–Scherrer equation ($D = 0.9\lambda/\beta \cos\theta$) [46]. The crystallite sizes for Fe_3O_4@SiO_2-NHCO-NH_2, Fe_3O_4@SiO_2-MnTCPP, Fe_3O_4@SiO_2-NH_2-MnTCPP, and Fe_3O_4@SiO_2-NHCO-NH_2-MnTCPP were calculated to be 26.5, 26.4, 30.6 and 33.3 nm respectively. Based on the results after porphyrin deposition, the average particle sizes of different supports were enhanced and crystallinity was decreased, which is attributed to the attachment of Mn-porphyrin onto the surface.

The magnetic properties of the prepared samples were evaluated by vibrating sample magnetometer (VSM) [44]. The saturated magnetization values of Fe_3O_4, Fe_3O_4@SiO_2, Fe_3O_4@SiO_2-NH_2, Fe_3O_4@SiO_2-NHCO-NH_2, Fe_3O_4@SiO_2-NHCO-NH_2-MnTCPP, Fe_3O_4@SiO_2-NH_2-MnTCPP, and Fe_3O_4@SiO_2-MnTCPP are 55, 41, 37, 34, 22, 27, 30 amu/g respectively (Fig. 5. a-g). The value of saturation magnetization of the nanocatalysts is lower than Fe_3O_4 nanoparticles, which should be ascribed to the existence of hybrid materials shells. The magnetization of nanocatalysts is sufficient to achieve complete separation with an external magnet [47, 48].

The morphology of the prepared nanocatalyst was studied by field emission scanning electron microscopy (FE-SEM). The uniformity and the smooth spherical morphology of magnetic nanoparticles Fe_3O_4@SiO_2-MnTCPP, Fe_3O_4@SiO_2-NHCO-NH_2, and Fe_3O_4@SiO_2-NHCO-NH_2-MnTCPP revealed in Fig. 6 (a, b and c) respectively, and some particles size were measured by random for Fe_3O_4@SiO_2-NHCO-NH_2, and Fe_3O_4@SiO_2-NHCO-NH_2-MnTCPP (SI. 2 a, b). The slight aggregation suggests the immobilization of a large amount of Mn porphyrin onto the surface of functionalized solid support (Fe_3O_4@SiO_2-NHCO-NH_2) (Fig. 6. c). Totally, proper particles size distribution could provide sufficient active site in the reaction [49–51].

Also, the morphology of synthesized catalysts was characterized by transmission electron microscope (TEM) analysis. As shown in Fig. 7a-c, the spherical morphology displayed a Fe_3O_4 core in the middle, which is protected by a thin shell of silica in Fe_3O_4@SiO_2-MnTCPP, Fe_3O_4@SiO_2-NH_2-MnTCPP, and Fe_3O_4@SiO_2-NHCO-NH_2-MnTCPP catalysts. A small changes in the morphology of the catalysts can be associated with the covalent linkage of the porphyrin onto magnetic support [29]. The core-shell size of Fe_3O_4@SiO_2-NHCO-NH_2-MnTCPP was measured by random, and19.4 nm and 10.15 nm for core and shell layers were calculated, respectively (SI. 3).

The thermal stability of the prepared nanocatalyst, Fe_3O_4@SiO_2-NHCO-NH_2-MnTCPP, was investigated through thermogravimetric analysis (TGA) under an O_2 atmosphere (100 ml/min) at the heating rate of 10℃/min in the range of ambient temperature up to 800°C (Fig. 8). The TGA spectrum showed the weight loss steps for the catalyst. As shown in Fig. 8, a weight loss observed at 150°C is due to the loss of water molecules, which are physically adsorbed on the surface of the catalyst [52]. The subsequent weight loss displayed at 180–290°C, which can be associated with the desorption of chemically bonded H_2O molecules to SiO_2. In the range of 300–800°C weight loss could be attributed to the decomposition of organic parts.

3. 2 Catalytic activities of magnetic nanocatalysts

The effectiveness of magnetic nanocatalyst Fe_3O_4@SiO_2-NHCO-NH_2-MnTCPP (C-3) was studied in the oxidation of different olefins. Cyclooctene was selected as a model substrate to optimize the reaction conditions. Some of the effective parameters in the reaction including solvent, temperature, and reaction time in the epoxidation reaction were evaluated. Molecular oxygen and isobutyraldehyde (IBA) were used as oxygen source and co-reactant, respectively. To investigate the effect of solvent on the catalytic oxidation of cyclooctene with O_2 in the presence of C-3 magnetic nanocatalyst, various solvents such as ethanol, methanol, acetone, acetonitrile, and the mixture of ethanol:dichloromethane (1:1 molar ratio) were applied. It was found that in the oxidation of cyclooctene with O_2 after 4 h in acetone (76%) and acetonitrile (78%) afforded the most efficiencies (Table. 1). It is worth noting that the solvent nature plays a major role in improving the activity of nanocatalyst [53]. The polarity and low coordination ability of acetonitrile and acetone are the effective properties that increase the total conversion in comparison with the others (MeOH or EtOH). Acetone was selected as the reaction solvent due to its abundance, economic advantage, and non-toxic properties. It should be noted that the epoxy cyclooctane was the main product (acetophenone and benzaldehyde were the other by-products).

To achieve more catalytic performance, magnetic nanocatalyst (C-3) was carried out in various reaction times, and temperatures and the results are shown in Fig. 9. After 2 hours, favored conversion was achieved in the presence of C-3 catalyst (61%) at room temperature. By continuing the reaction for up to 3 hours at ambient temperature, the oxidation reaction boosted up to 70%. Since the temperature is a crucial parameter in the oxidation of olefins with molecular oxygen, the effect of temperature on the oxidation reaction of cyclooctene with O_2 in the presence of magnetic nanocatalyst (C-3) in acetone was studied (Fig. 9). Based on the results, low temperature had a negative effect and low conversion of epoxy cyclooctane was achieved after 3 hours at 5°C (8%). By increasing the temperature to 25°C, Mn-catalyst shows higher catalytic performance after 3 hours (70%). The catalytic efficiency of Fe_3O_4@SiO_2-NHCO-NH_2-MnTCPP (C-3) improved with a slight increase in temperature. After 3 hours, the desirable result (85%) was obtained for the oxidation reaction of cyclooctene in the presence of catalyst at 38℃±2 (Fig. 9).

Aim to a comparison study under obtained optimum reaction condition, the catalytic performance of Fe_3O_4@SiO_2-MnTCPP (C-1), Fe_3O_4@SiO_2-NH_2-MnTCPP (C-2), and Fe_3O_4@SiO_2-NHCO-NH_2-MnTCPP (C-3)

were investigated toward different types of olefins (Table 2). The oxidation of olefins proceeded well and the major product of the oxidation of olefins with O_2 in the presence of Mn nanocatalysts was the corresponding epoxides. Accordingly, excellent conversions and selectivity to epoxide was attained for all olefins in the presence of the newly synthesized catalyst, Fe_3O_4@SiO_2-NHCO-NH_2-MnTCPP (C-3). In other words, the results illustrated the superiority of the newly designed linker over catalytic performance. The current catalytic system (C-3) led to the complete conversion of α-methyl styrene, 4-methyl styrene, and 4-chloro styrene after two hours (Table 2, entries 1–3). The catalysts could oxidize even the linear terminal alkenes such as 1-hexene and 1-octene (Table 2, entries 9, 10). Fortunately, the new designed catalyst (C-3) was the superior catalyst through C-1, C-2, in the oxidation of all cases of olefins in the presence of O_2after two hours.

Table 1

Effect of solvent on the oxidation of styrene with O_2 in the presence of C-3 catalyst at room temperature.[a]

Entry	Solvent	Conversion %[b]	TON
1	Methanol	16	16
2	Ethanol	14	14
3	Acetone	76	76
4	Acetonitrile	78	78
5	Ethanol: Dichlorometane	43	43

[a]The molar ratios for Catalyst C-3: ImH: Cyclooctene: IBA are (1:100:100:500) under an oxygen atmosphere for 4 h. [b]Based on starting material.

To evaluate the reusability and stability of Fe_3O_4@SiO_2-NHCO-NH_2-MnTCPP (C-3), Fe_3O_4@SiO_2-NH_2-MnTCPP (C-2), and Fe_3O_4@SiO_2-MnTCPP (C-1), the oxidation of styrene was examined in six reaction cycles under the optimized conditions. At the end of each reaction run, the C-1, C-2, and C-3 catalysts were separated from the reaction mixture by external magnet, washed thoroughly with ethanol and acetone to get rid of the organic reactant molecules and dried at 60 ℃, then directly used in the next run. All catalysts were reused in repeated epoxidation reactions with fresh reactants (Fig. 10). Based on the results, the prepared magnetic nanocatalyst with the long linker length (C-3) showed excellent reusability after seven consecutive cycles with little loss of activity. In contrast, the catalytic activity of the short or medium linker length (C-2 and C-3) decreased after three cycles of use. The FT-IR spectra and FE-SEM of the final cycle of reuse correspond to C-3, showing no significant difference in the structure of the reused catalyst versus the fresh catalyst (Fig. 11. a, b). This investigation confirmed that Fe_3O_4@SiO_2-NHCO-NH_2-MnTCPP (C-3) is the most stable and recyclable heterogeneous catalyst in comparison with Fe_3O_4@SiO_2-MnTCPP (C-1) and Fe_3O_4@SiO_2-NH_2-MnTCPP (C-2).

To investigate the catalytic performance of the prepared catalysts, a blank experiment was also performed and the result showed that the presence of catalyst (C-3) and isobutyraldehyde is essential for an efficient catalytic reaction and in the absence of the catalyst, only 14% cyclooctene oxide was obtained. Also, in the presence of MnTCPP as a catalyst, 25% conversion was observed (Table 3).

Table 3
The oxidation of cyclooctene in various conditions.

Entry	Catalyst (mmol)	Condition	Conversion %
1	None	-------	14
2	MnTCPP	-------	25
3	Fe_3O_4@SiO_2-NHCO-NH_2-MnTCPP	IBA free	Trace
4	Fe_3O_4@SiO_2-NHCO-NH_2-MnTCPP	Optimum	72
Reaction condition: Catalyst:substrate:IBA (1:100:500), acetone:1 ml, 38°C±2, 2 h. Based on $15_{\square}10^{-4}$ mmol of the catalyst.			

The present work has been compared with some recently reported articles in the oxidation of cyclooctene to evaluate the catalytic performance of the prepared nanocatalyst. As shown in Table 4, reasonable reaction time and utilizing green oxidant (O_2) for oxidation of cyclooctene in the mild condition are significant advantages of the C-3 catalyst compared to some recently reported data.

Table 4
Comparison of literature reports of MNPs catalysts on the oxidation of cyclooctene under various conditions.

Entry	Catalyst	Oxidant	solvent	T(h)/Tem. °C	Conversion %	Ref.
1	MNP@SiO_2[4-NH-Mn-TDCPP]	O_2	C_3H_7CN	3.5/25	99	[54]
2	Fe_3O_4@SiO_2-N3@[MnTHPP]	TBHP	$C_2H_4Cl_2$	12/75	95	[41]
3	Fe3O4@SiO2 -CPS-L-MoO2 (EtOH)	TBHP	$C_2H_4Cl_2$	4/reflux	100	[50]
4	Fe_3O_4/SiO_2/NH_2-Mn(TCPP)OAc	H_2O_2	CH_3CN	5/25	87	[28]
5	Fe_3O_4@MCM-41-Im@MnPor	$NaIO_4$	CH_3CN/H_2O	2/25	98	[40]
6	Fe_3O_4@SiO_2-NHCO-NH_2-MnTCPP (C-3)	O_2	Acetone	3/38	99	Present work

A probable mechanism for the epoxidation of cyclooctene by C-3 with O_2 has been illustrated in Scheme 2. Based on the literature, isobutyraldehyde as a useful reducing agent for aerobic oxidations with O_2 plays an important role in the oxidation reaction [50, 51]. In the catalytic oxidation of olefins with molecular O_2/IBA, free radicals are involved. Generally, the generated acyl radical reacts with dioxygen to give an acylperoxy radical. During the reaction between an acylperoxy radical with another aldehyde, peroxyisobutyric acid will be produced. By continuing the reaction, a high valent Mn-oxo species formed, which are responsible for oxygen transfer (Scheme 2).

4 Conclusions

In summary, recyclable superparamagnetic nanocatalysts, C-1, C-2, and C-3, were synthesized by immobilizing of MnTCPP to amino functionalized silica-coated MNPs. The catalytic activity of prepared catalysts was evaluated and compared in the green oxidation of various olefins with molecular oxygen. The distinct point of prepared catalysts (Fe_3O_4@SiO_2-NHCO-NH_2-MnTCPP (C-3), Fe_3O_4@SiO_2-NH_2-MnTCPP (C-2), and Fe_3O_4@SiO_2-MnTCPP (C-1)) is the linker length, which anchored the MnTCPP on to the surface of support. The obtained results were demonstrated that the catalytic activity and stability of Mn-porphyrins are significantly improved by immobilization onto the surface of magnetic nanoparticles with a long linker length.

Declarations

Acknowledgement

The authors are thankful to the Graduate Study Councils of Shahid Beheshti University and K. N. Toosi University of Technology for financial support of this research.

Data Availability

The data that support the findings of this study are available in the supplementary material of this article.

Conflict of interest There are no conflict to declare.

References

1. G. De Faveri, G. Ilyashenko, M. Watkinson, Chem. Soc. Rev. **40**, 1722 (2011)
2. X. Jing, D. Yuan, L. Yu, Adv. Synth. Catal. **359**, 1194 (2017)
3. M. Sankaralingam, M. Balamurugan, M. Palaniandavar, Coord. Chem. Rev. **403**, 213085 (2020)
4. O.C. Williams, C. Sievers, Appl. Catal. A **614**, 118057 (2021)
5. J.P. Kehrer, J.D. Robertson, C.V. Smith, C.A. McQueen (eds.), *Comprehensive Toxicology*, 2nd edn. (Elsevier, Oxford, 2010)
6. H. Tanaka, H. Nishikawa, T. Uchida, T. Katsuki, J. Am. Chem. Soc. **132**, 12034 (2010)

7. S. Rayati, N. Pournaser, F. Nejabat, P. Nafarieh, Inorg. Chem. Commun. **107**, 107447 (2019)
8. L. Fu, Y. Lu, Z. Liu, R. Zhu, Chin. J. Catal. **37**, 398 (2016)
9. A. Zarrinjahan, M. Moghadam, V. Mirkhani, S. Tangestaninejad, I. Mohammadpoor-Baltork, J Iran. Chem Soc **13**, 1509 (2016)
10. M. Kazemnejadi, A. Shakeri, M. Nikookar, M. Mohammadi, M. Esmaeilpour, Res. Chem. Intermed **43**, 6889 (2017)
11. Z. Špitalský, C.A. Krontiras, S.N. Georga, C. Galiotis, Compos. Part A **40**, 778 (2009)
12. M. Kathalewar, A. Sabnis, J. Coat. Technol. Res. **11**, 601 (2014)
13. K.C.M. Westrup, R.M. da Silva, K.M. Mantovani, L. Bach, J.F. Stival, P.G.P. Zamora, F. Wypych, G.S. Machado, S. Nakagaki, Appl. Catal. A **602**, 117708 (2020)
14. N. Ananthi, I.V.M.V. Enoch, Chirality. **31**, 155 (2019)
15. X.-X. Guo, J. Jiang, Q. Han, X.-H. Liu, X.-T. Zhou, H.-B. Ji, Appl. Catal. A **590**, 117352 (2020)
16. S. Shokoohi, S. Rayati, J. Porphyrins Phthalocyanines **26**, 8 (2022)
17. F. Nejabat, S. Rayati, J. Ind. Eng. Chem. **69**, 324 (2019)
18. L.Brown Jeff, Civ. Eng. Mag Arch. **85**, 50 (2015)
19. J.T. Groves, P.R. Ortiz, de Montellano (eds.), *Cytochrome P450: Structure, Mechanism, and Biochemistry* (Springer US, Boston, 2005)
20. K. Berijani, A. Farokhi, H. Hosseini-Monfared, C. Janiak, Tetrahedron. **74**, 2202 (2018)
21. E. Maligaspe, A.S.D. Sandanayaka, T. Hasobe, O. Ito, F. D'Souza, J. Am. Chem. Soc. **132**, 8158 (2010)
22. K. Hemmat, M.A. Nasseri, A. Allahresani, Appl. Organomet. Chem. **33**, e4937 (2019)
23. K. Manjunatha, T.S. Koley, V. Kandathil, R.B. Dateer, G. Balakrishna, B.S. Sasidhar, S.A. Patil, S.A. Patil, Appl. Organomet. Chem. **32**, e4266 (2018)
24. I. Kuźniarska-Biernacka, C. Pereira, A.P. Carvalho, J. Pires, C. Freire, Appl. Clay Sci. **53**, 195 (2011)
25. D. Zhao, J. Zhao, S. Zhao, W. Wang, J. Inorg. Organomet. Polym. Mater. **17**, 653 (2007)
26. H. Zhang, Y.M. Wang, L. Zhang, G. Gerritsen, H.C.L. Abbenhuis, R.A. van Santen, C. Li, J. Catal. **256**, 226 (2008)
27. L. Hadian-Dehkordi, H. Hosseini-Monfared, P. Aleshkevych, Inorg. Chim. Acta **462**, 142 (2017)
28. S. Rayati, D. Moradi, F. Nejabat, New. J. Chem. **44**, 19385 (2020)
29. S. Rayati, F. Nejabat, F. Panjiali, Catal. Commun. **122**, 52 (2019)
30. L. Cheng, D. Jiang, A. Kamkaew, H.F. Valdovinos, H.-J. Im, L. Feng, C.G. England, S. Goel, T.E. Barnhart, Z. Liu, W. Cai, Adv. Funct. Mater. 1702928 (2017)
31. N. Sharma, S.S. Dhankhar, C.M. Nagaraja, Microporous Mesoporous Mater. **280**, 372 (2019)
32. S. Shanmugam, S. Krishnaswamy, R. Chandrababu, U. Veerabagu, A. Pugazhendhi, T. Mathimani, Fuel. **273**, 117777 (2020)
33. M. Amblard, J.-A. Fehrentz, J. Martinez, G. Subra, Mol. Biotechnol. **33**, 239 (2006)

34. A. Ghodrati, L. Firoozpour, S. Balalaie, F.S. Hosseini, S. Ramezanpour, N. Edraki, N. Mohtavinejad, M. Amanlou, Int. J. Pept. Res. Ther. **26**, 2169 (2020)
35. I. Banerjee, K.C. Ghosh, E. Oheix, M. Jean, J.-V. Naubron, M. Réglier, O. Iranzo, S. Sinha, The J. Org. Chem. **86**, 2210 (2021)
36. I.E. Sampaio-Dias, C.A.D. Sousa, S.C. Silva-Reis, S. Ribeiro, X. García-Mera, J.E. Rodríguez-Borges, Org. Biomol. Chem. **15**, 7533 (2017)
37. Z. Liu, B.-H. Hu, P.B. Messersmith, Tetrahedron Lett. **49**, 5519 (2008)
38. B. Zhou, Y. Tang, L. Zhao, L. Guo, J. Zhou, RSC Adv. **11**, 1172 (2021)
39. I. Elsayed, M. Mashaly, F. Eltaweel, M.A. Jackson, Fuel. **221**, 407 (2018)
40. R. Hajian, A. Ehsanikhah, Chem. Phys. Lett. **691**, 146 (2018)
41. M. Bagherzadeh, M. Hosseini, A. Mortazavi-Manesh, Inorg. Chem. Commun. **107**, 107495 (2019)
42. G. Piccirillo, M. Moreira-Santos, M. Válega, M.E.S. Eusébio, A.M.S. Silva, R. Ribeiro, H. Freitas, M.M. Pereira, M.J.F. Calvete, Appl. Catal. B **282**, 119556 (2021)
43. T. Mokary Yazdely, M. Ghorbanloo, H. Hosseini-Monfared, New. J. Chem. **43**, 11926 (2019)
44. F. Ghorbani, S. Kamari, Environ. Technol. Innovation **14**, 100333 (2019)
45. K. Urbanska, M. Pawlicki, J. Org. Chem. **85**, 8196 (2020)
46. K. He, N. Chen, C. Wang, L. Wei, J. Chen, Cryst. Res. Technol. **53**, 1700157 (2018)
47. A. Bagherpour, F. Kashanian, S.S. Ebrahimi, M. Habibi-Rezaei, J. Nanotechnol **29**, 075706 (2018)
48. S.A.A. Noma, A. Ulu, S. Koytepe, B. Ateş, Biocatal. Biotransform. **38**, 392 (2020)
49. M. Ece, A. Ekinci, S. Kutluay, Ö Şahin, S. Horoz, J. Mater. Sci. : Mater. Electron. **32**, 18192 (2021)
50. M. Sarkheil, M. Lashanizadegan, Appl. Organomet. Chem. **32**, e4459 (2018)
51. D. Ren, S. Jiang, L. Fu, Z. Wang, S. Zhang, X. Zhang, X. Gong, W. Chen, Environ. Technol. **42**, 1 (2021)
52. S. Rayati, E. Khodaei, P. Nafarieh, M. Jafarian, B. Elmi, A. Wojtczak, RSC Adv. **10**, 17026 (2020)
53. M. Kazemnejadi, B. Mahmoudi, Z. Sharafi, M.A. Nasseri, A. Allahresani, M. Esmaeilpour, J. Organomet. Chem. **896**, 59 (2019)
54. L.D. Dias, R.M.B. Carrilho, C.A. Henriques, G. Piccirillo, A. Fernandes, L.M. Rossi, M. Filipa Ribeiro, M.J.F. Calvete, M.M. Pereira, J. Porphyrins Phthalocyanines **22**, 331 (2018)

Tables

Table 2 is available in the Supplementary Files section

Scheme

Schemes 1 & 2 are available in the Supplementary Files section.

Figures

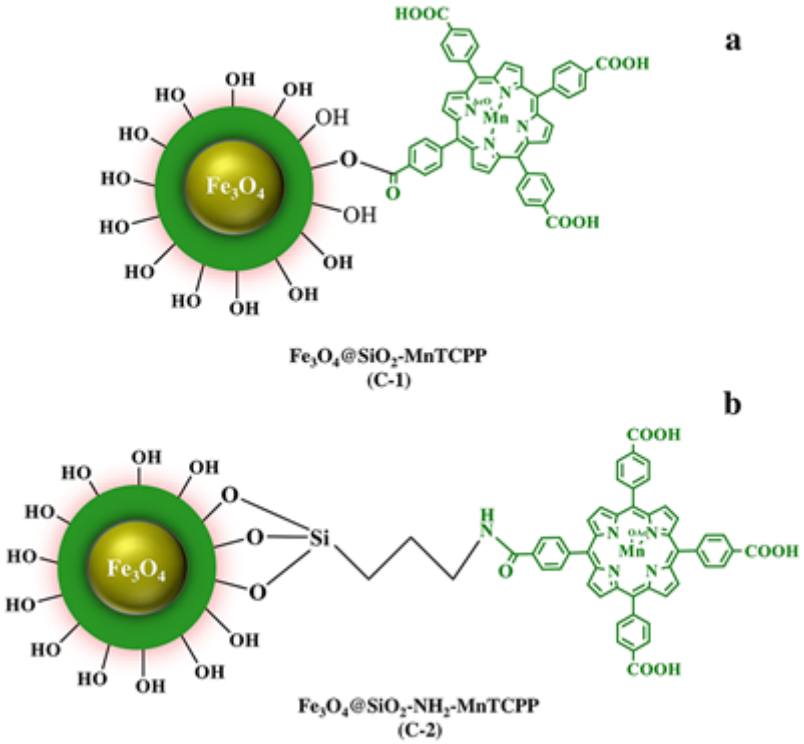

Figure 1

The schematic illustration of C-1 and C-2 catalysts.

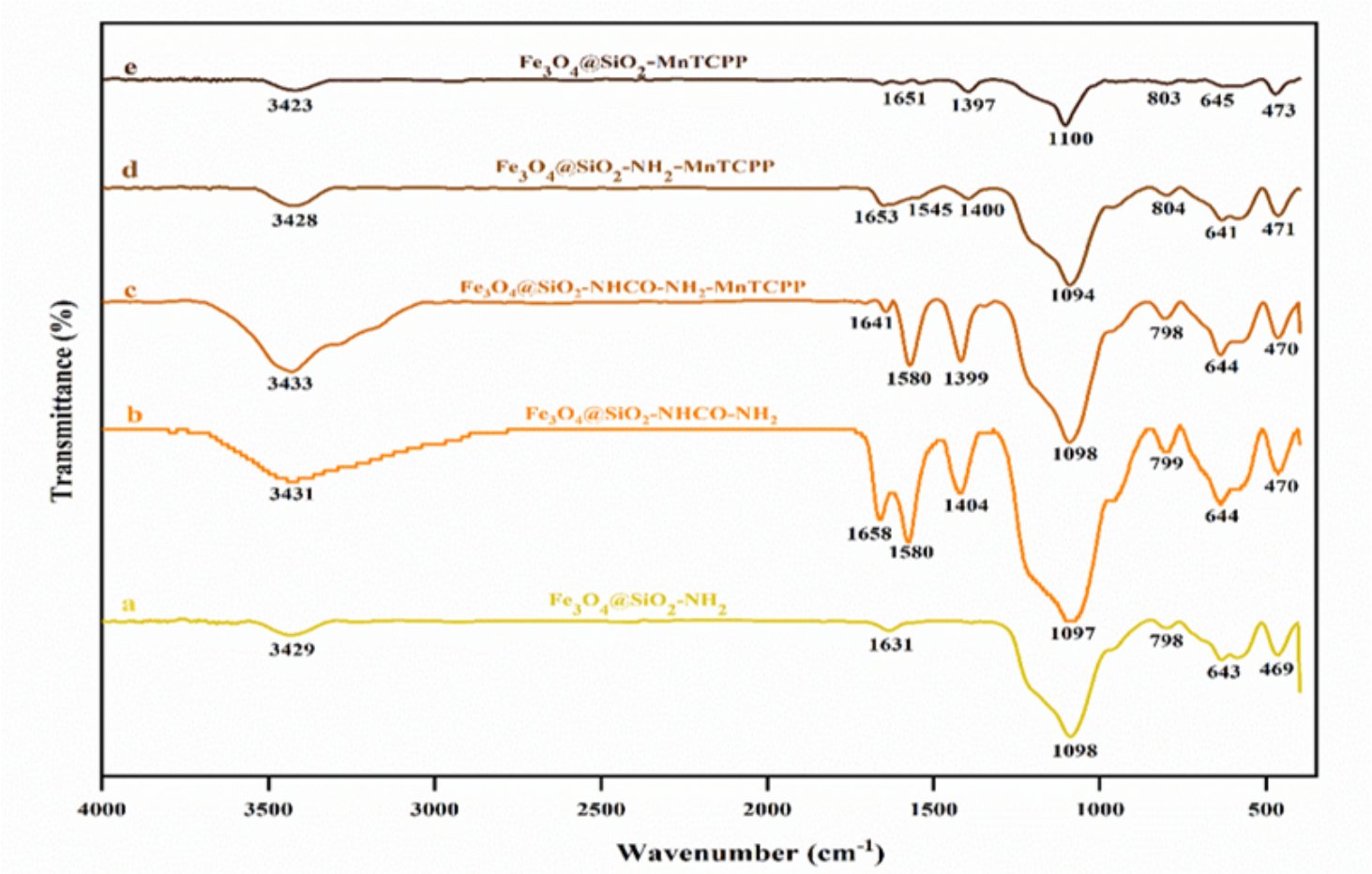

Figure 2

The FT-IR spectra of Fe_3O_4@SiO_2-NH_2 (a), Fe_3O_4@SiO_2-NHCO-NH_2 (b), Fe_3O_4@SiO_2-NHCO-NH_2-MnTCPP (c), Fe_3O_4@SiO_2-NH_2-MnTCPP (d), Fe_3O_4@SiO_2-MnTCPP (e).

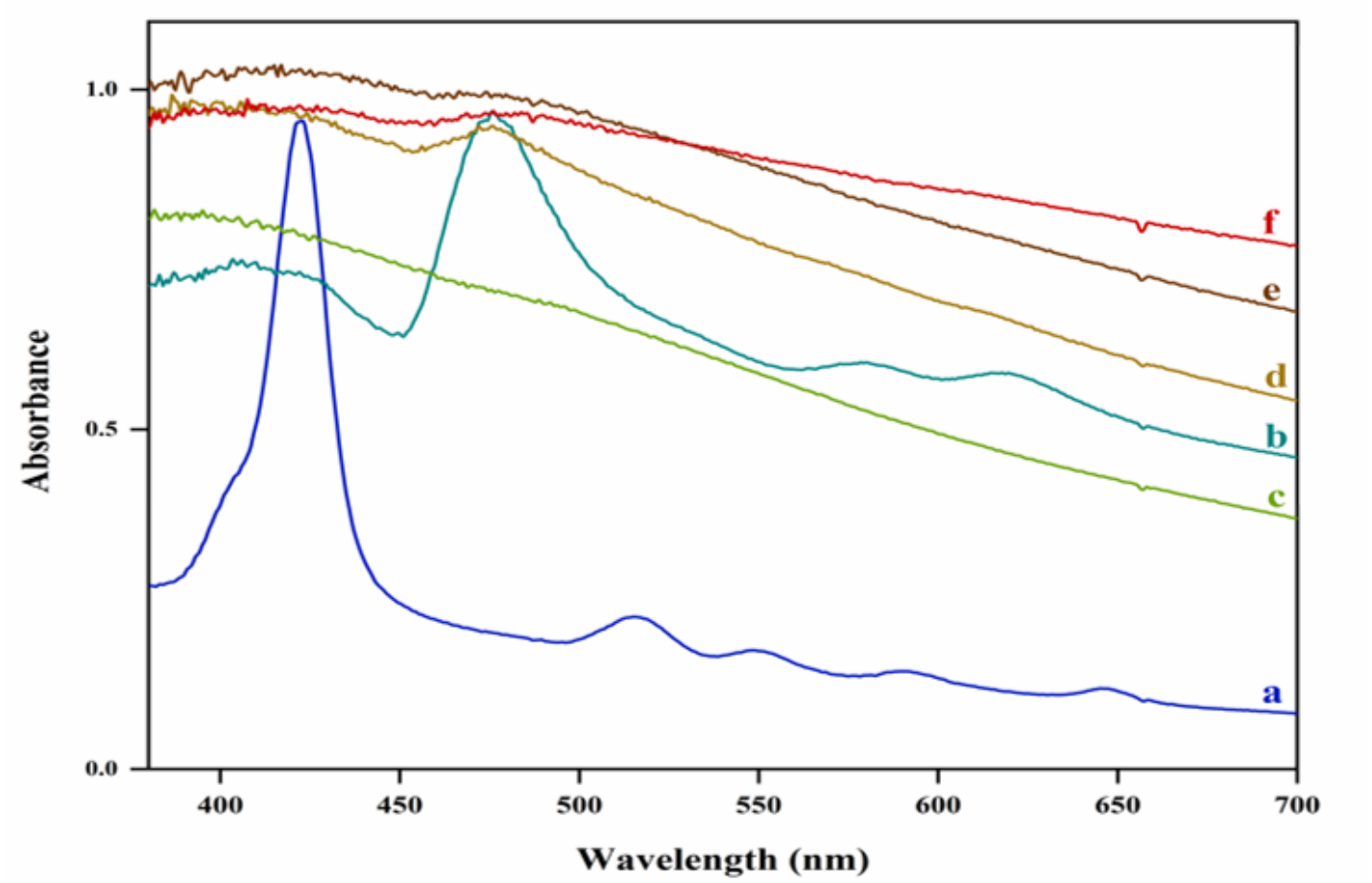

Figure 3

UV-Vis spectra of H_2TCPP (a), MnTCPP(OAc) (b), $Fe_3O_4@SiO_2$-NHCO-NH_2 (c), $Fe_3O_4@SiO_2$-NHCO-NH_2-MnTCPP (d), $Fe_3O_4@SiO_2$-NH_2-MnTCPP (e), $Fe_3O_4@SiO_2$-MnTCPP (f).

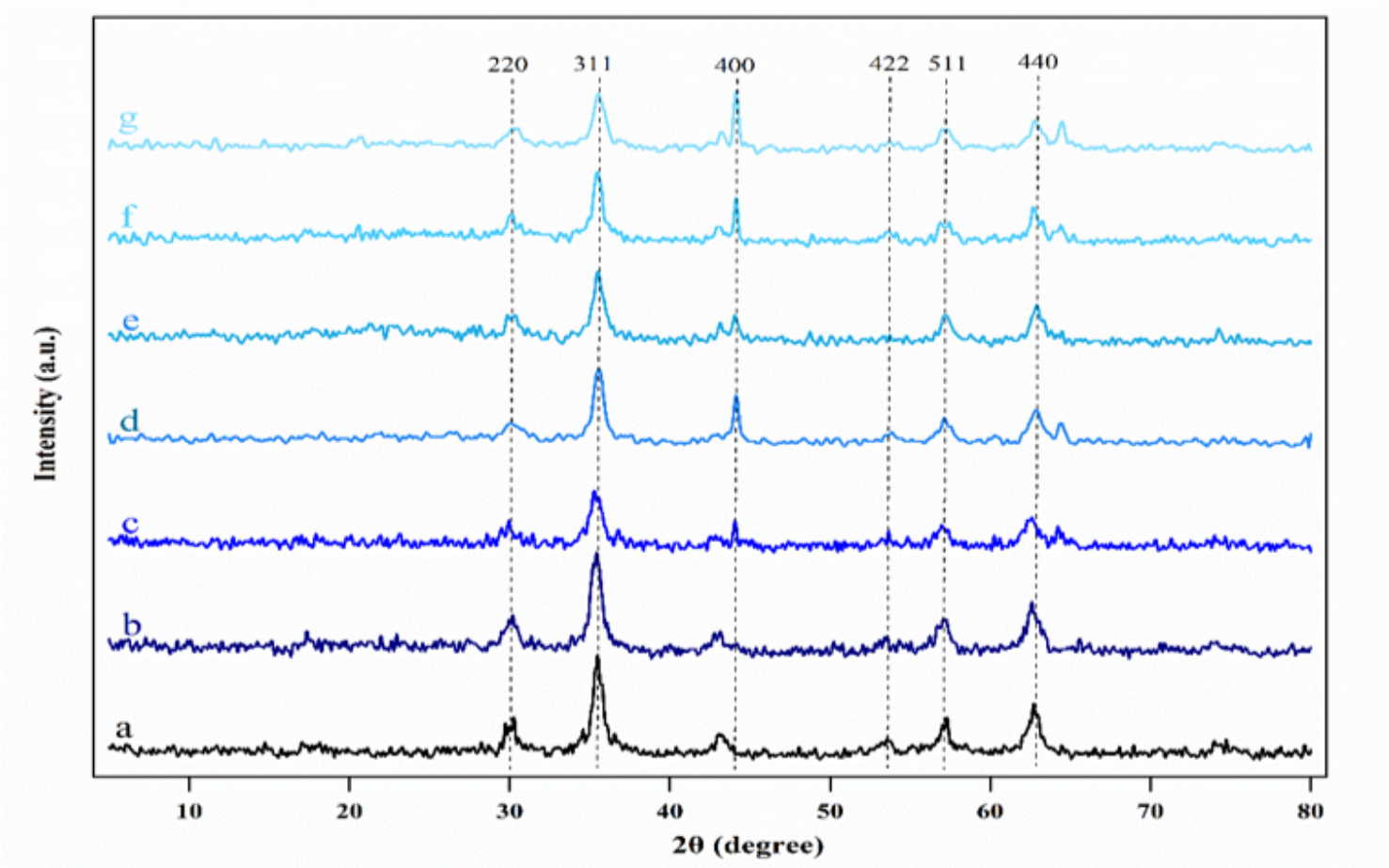

Figure 4

XRD pattern of Fe_3O_4 (a), Fe_3O_4@SiO_2 (b), Fe_3O_4@SiO_2-NH_2 (c), Fe_3O_4@SiO_2-NHCO-NH_2 (d), Fe_3O_4@SiO_2-MnTCPP (e), Fe_3O_4@SiO_2-NH_2-MnTCPP (f) and Fe_3O_4@SiO_2-NHCO-NH_2-MnTCPP (g).

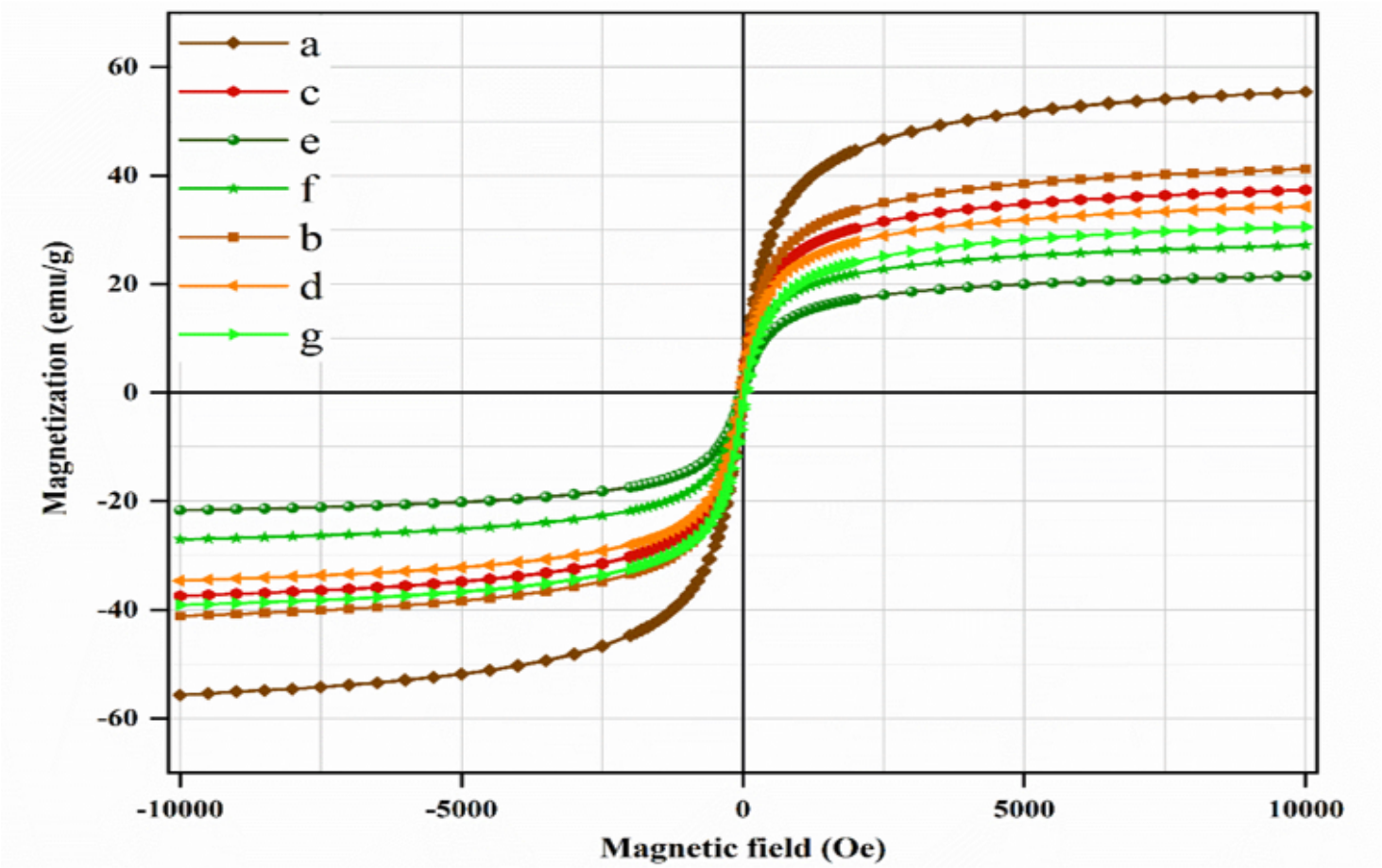

Figure 5

The VSM analysis of Fe_3O_4 (a), Fe_3O_4@SiO_2 (b), Fe_3O_4@SiO_2-NH_2 (c), Fe_3O_4@SiO_2-NHCO-NH_2 (d), C-3 (e), C-2 (f) C-1 (g).

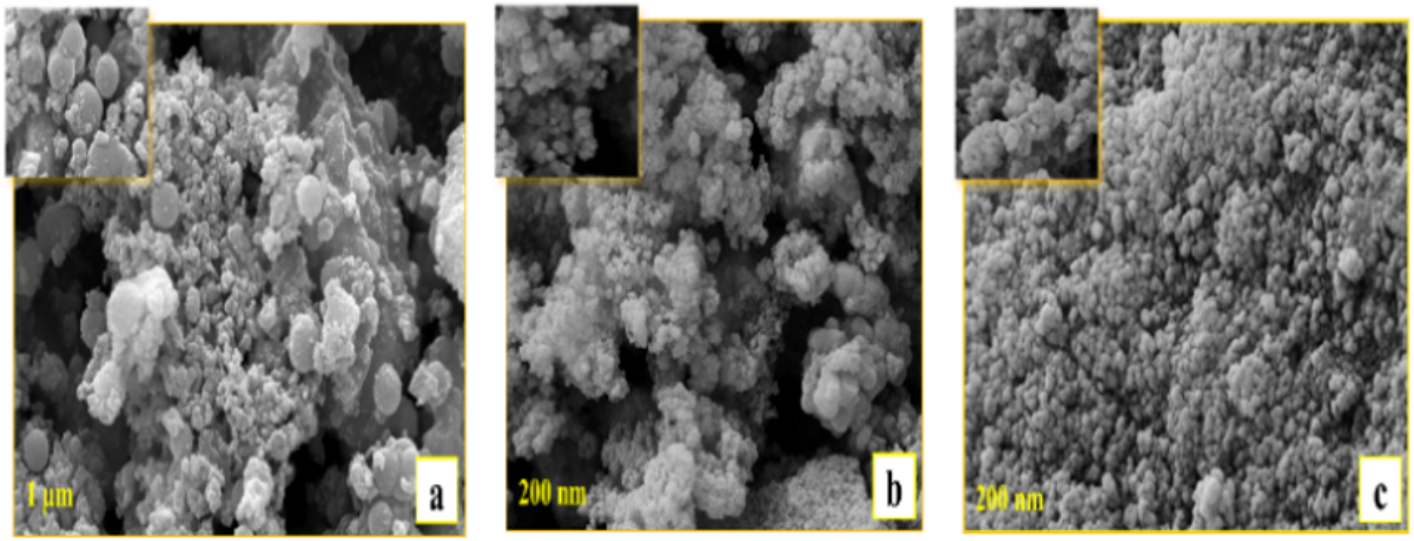

Figure 6

The FE-SEM images of Fe_3O_4@SiO_2-MnTCPP (a), Fe_3O_4@SiO_2-NHCO-NH_2 (b), and Fe_3O_4@SiO_2-NHCO-NH_2-MnTCPP (c).

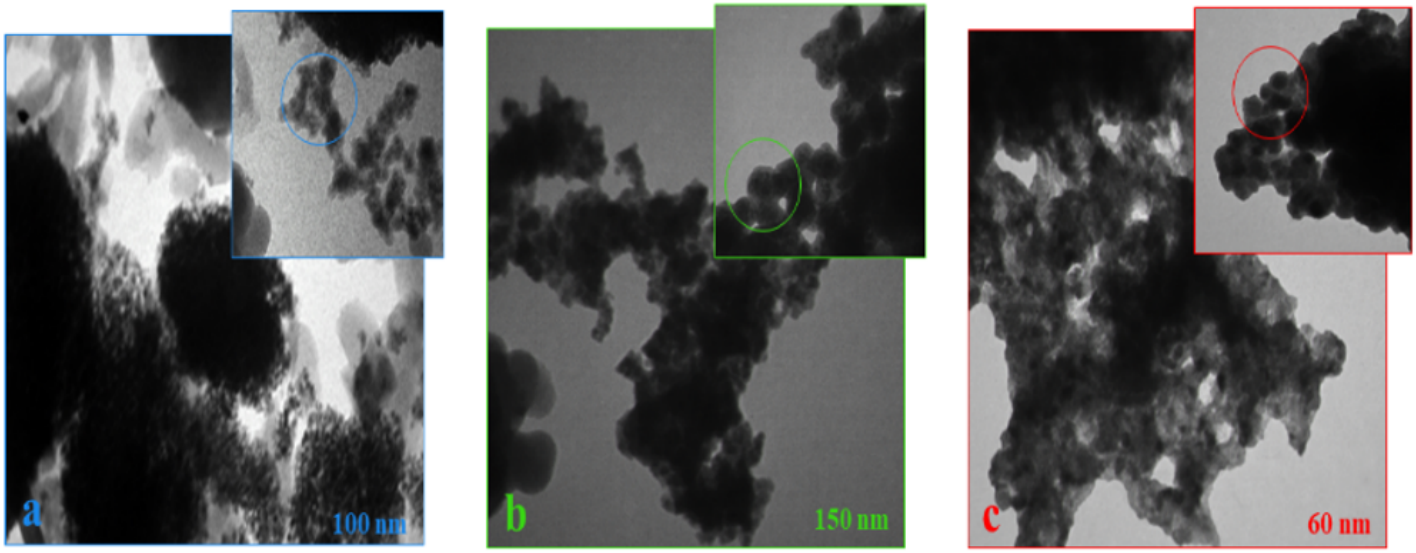

Figure 7

The TEM image of Fe_3O_4@SiO_2-MnTCPP (a), and Fe_3O_4@SiO_2-NH_2-MnTCPP (b), and Fe_3O_4@SiO_2-NHCO-NH_2-MnTCPP (c).

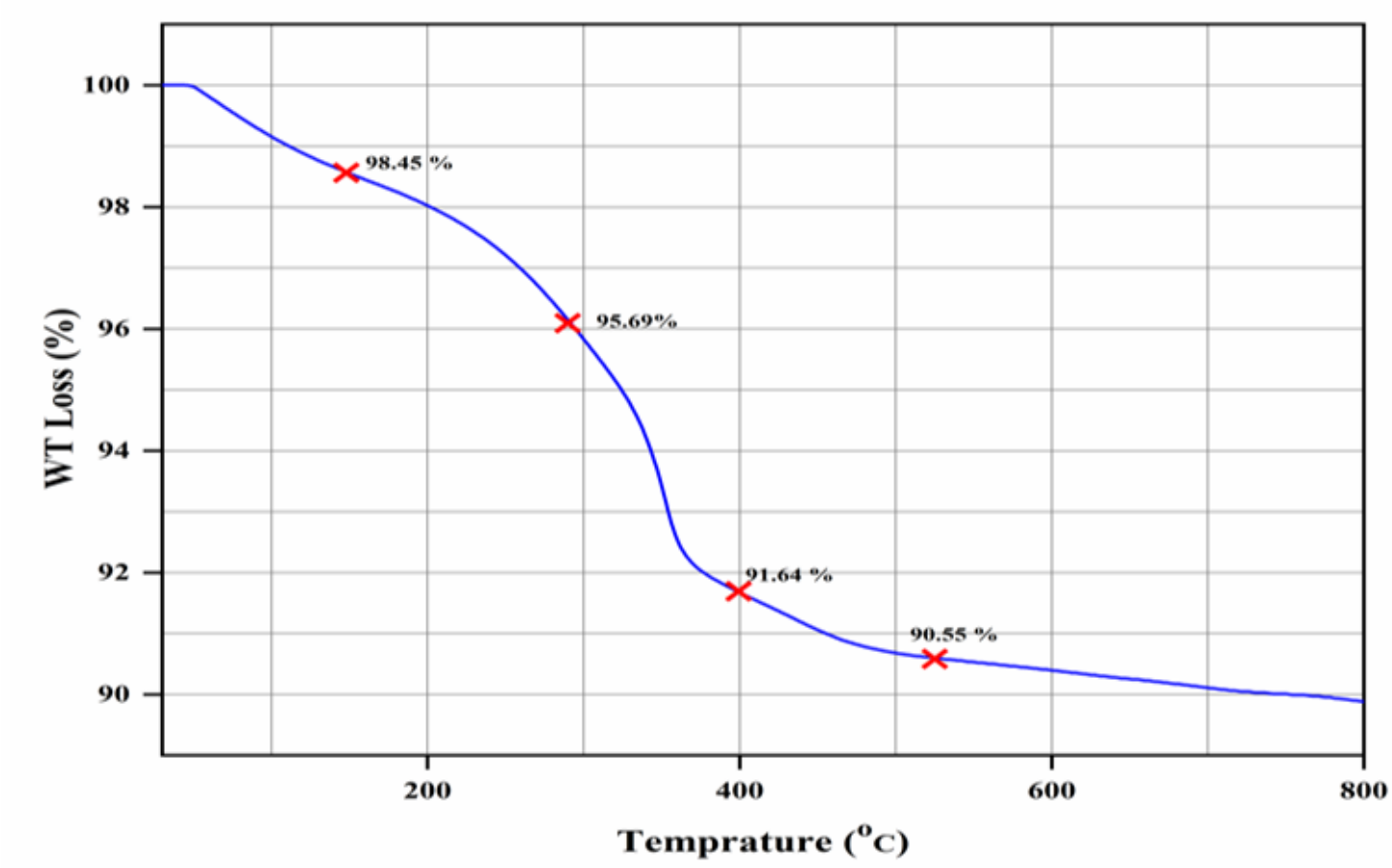

Figure 8

The thermogravimetric curve of Fe_3O_4@SiO_2-NHCO-NH_2-MnTCPP.

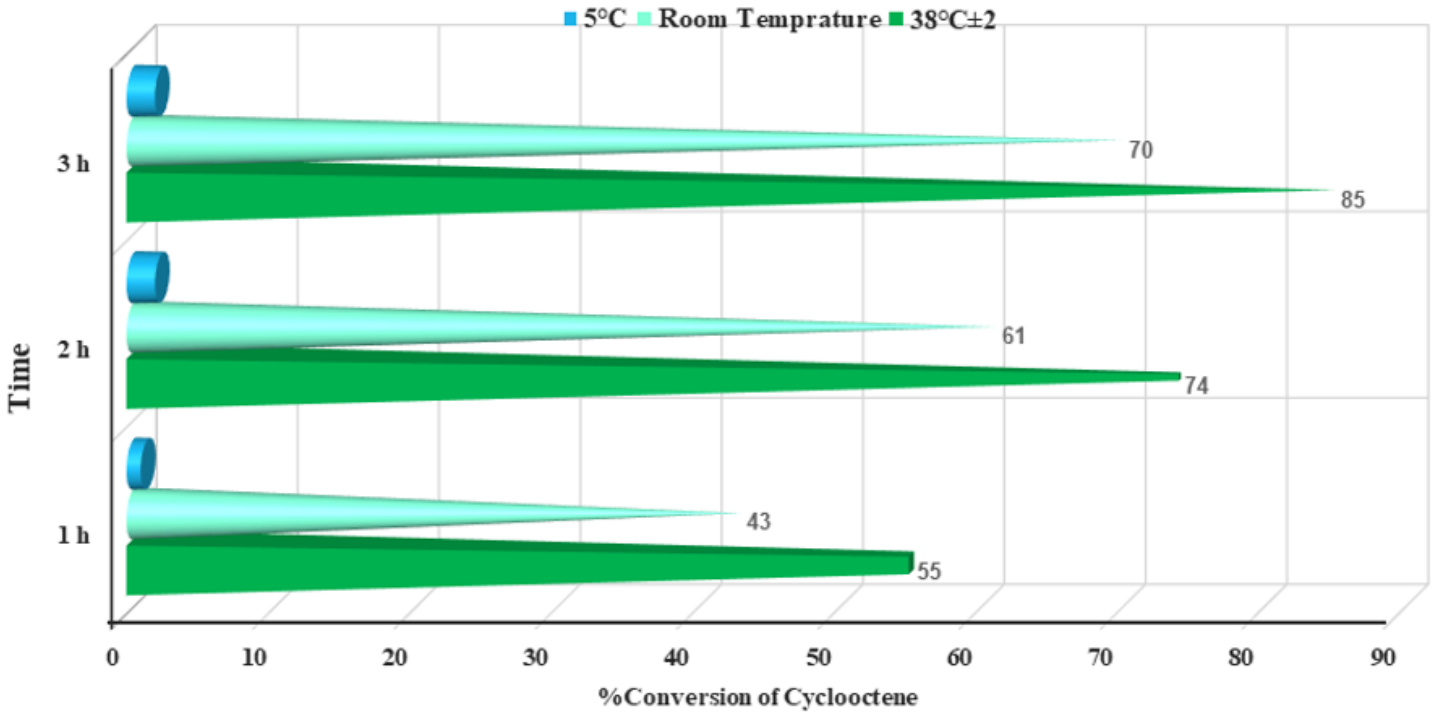

Figure 9

The effect of time and temperature on the oxidation of cyclooctene via O_2 in the presence of magnetic nanocatalyst C-3. Reaction condition: the molar ratio of Catalyst:ImH:Cyclooctene:IBA is (1:100:100:500), acetone (1 ml).

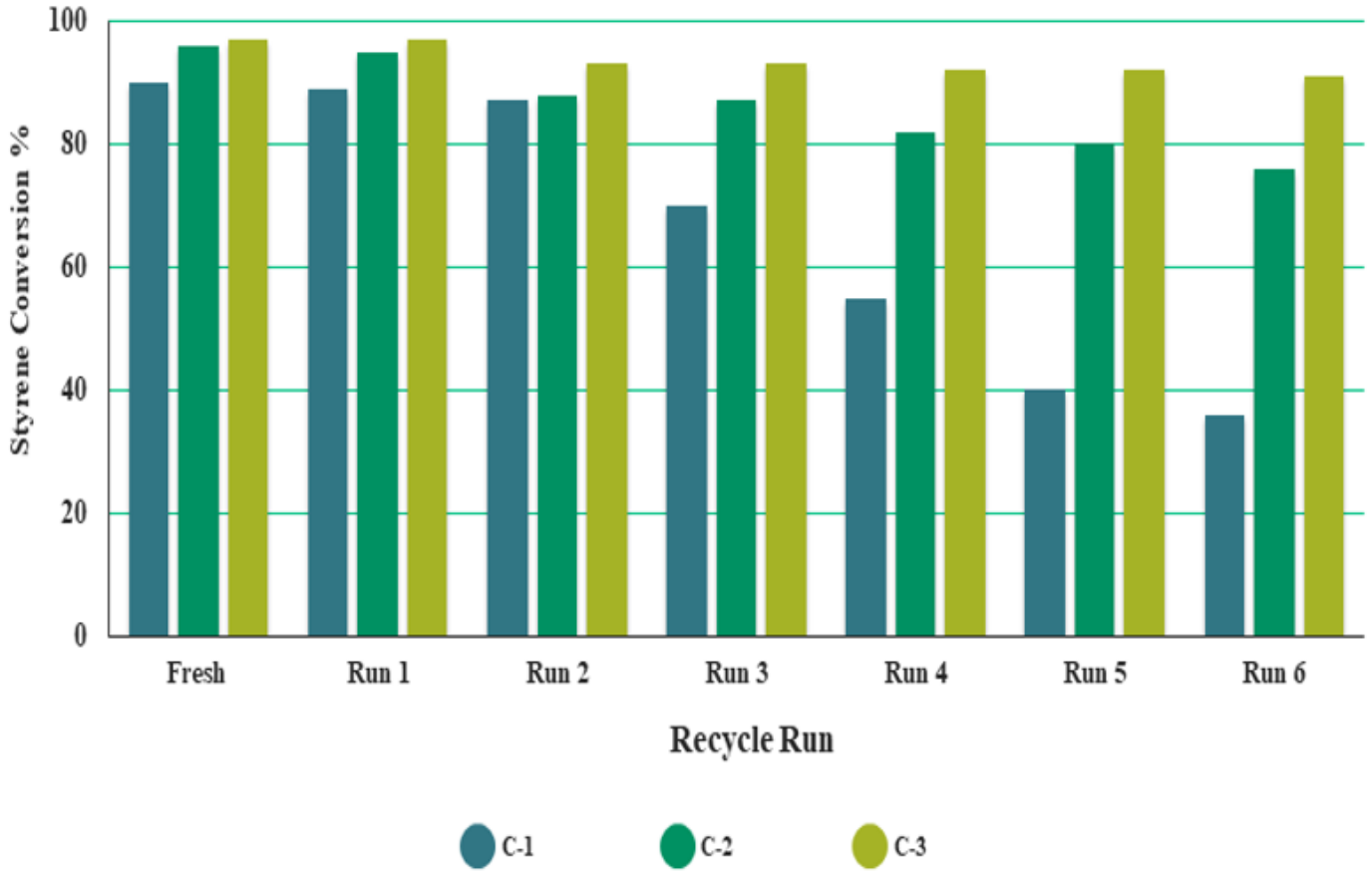

Figure 10

The recyclability of catalysts. Reaction condition: Cat: Sty: IBA (1:100:500), O_2, 1 ml Acetone, 2h, 38°C±2. Based on $15_{\square}10^{-4}$ mmol of catalyst.

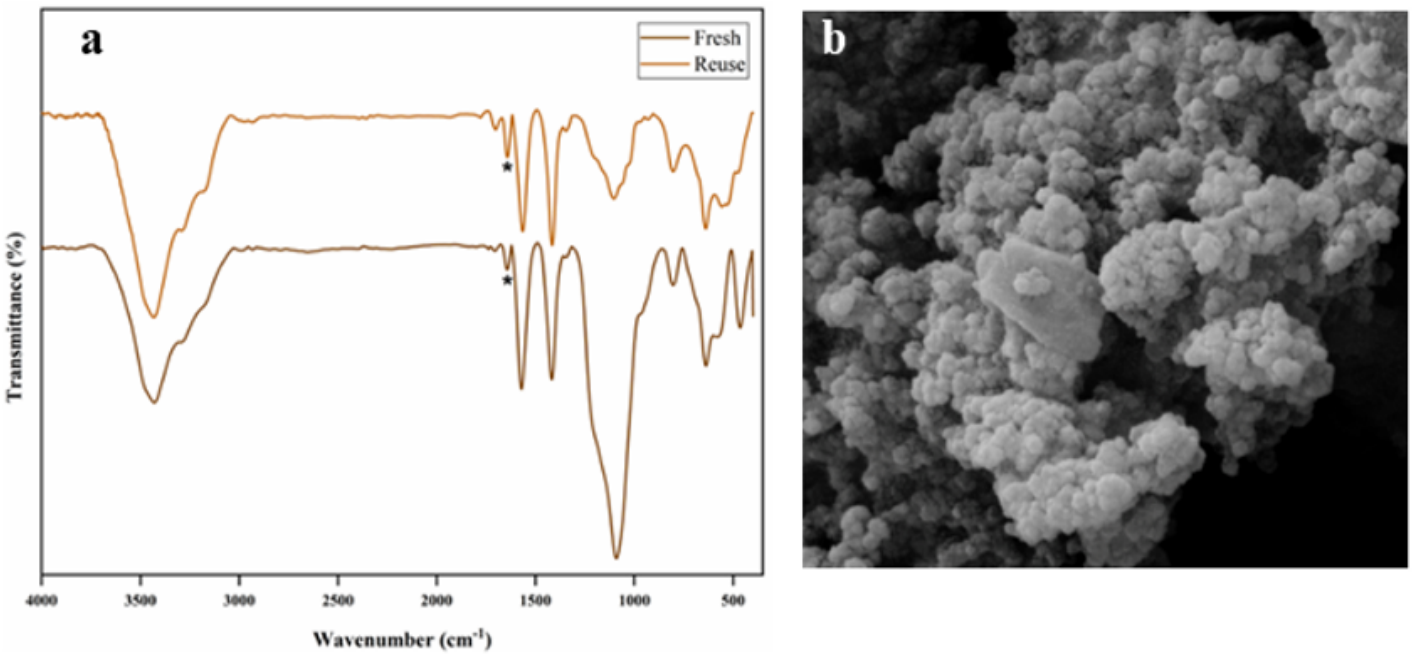

Figure 11

(a) FT-IR spectra and (b) FE-SEM image of Fe_3O_4@SiO_2-NHCO-NH_2-MnTCPP in last reuse cycle.

Supplementary Files

This is a list of supplementary files associated with this preprint. Click to download.

- Scheme1.png
- Scheme2.png
- SupportingInformationSI.docx
- Table2.docx